Acta Crystallographica Section D
Biological Crystallography
ISSN 1399-0047

Structures of *Legionella pneumophila* NTPDase1 in complex with polyoxometallates

Matthias Zebisch,[a,b]* Michel Krauss,[a] Petra Schäfer[a]‡ and Norbert Sträter[a]*

[a]Institute of Bioanalytical Chemistry, Center for Biotechnology and Biomedicine, University of Leipzig, Deutscher Platz 5, 04103 Leipzig, Germany, and [b]Division of Structural Biology, University of Oxford, Roosevelt Drive, Oxford OX3 7BN, England

‡ Present address: Department for Cell and Metabolic Biology, Leibniz Institute of Plant Biochemistry, 06120 Halle (Saale), Germany.

Correspondence e-mail: matthias@strubi.ox.ac.uk, strater@bbz.uni-leipzig.de

Received 24 August 2013
Accepted 27 January 2014

PDB references: NTPDase1, complexes with polyoxometallates, 4brh; 4bvo; 4bvp

Nucleoside triphosphate diphosphohydrolases (NTPDases) are secreted or membrane-bound ectonucleotidases that hydrolyze the anhydride bonds of nucleoside triphosphates and nucleoside diphosphates. Mammalian cell-surface NTPDase enzymes are inhibited by various polyoxometallates. Here, the structures of NTPDase1 from the bacterium *Legionella pneumophila* (*Lp*NTPDase1) in complex with the dodecatungstate POM-1, decavanadate and octamolybdate/heptamolybdate are described. The metal clusters are bound at different sites but always in a highly ordered fashion *via* electrostatic interactions and hydrogen bonds. For octamolybdate, covalent interactions after oxygen ligand exchange by a serine and histidine side chain are also observed. The potential inhibitory mechanism and the use of the metal clusters as phasing tools for new NTPDase structures are discussed. The binding mode of a tartrate ion at the catalytic centre suggests novel strategies for the structure-based design of NTPDase inhibitors, and the observation of the enzyme in an intermediate open state contributes to our understanding of NTPDase enzyme dynamics.

1. Introduction

NTPDases are a class of ectonucleotidases that are distributed ubiquitously among eukaryotes (Zimmermann *et al.*, 2012). In a divalent metal ion-dependent fashion, they catalyze the stepwise removal of the γ- and β-phosphates from nucleoside triphosphates and diphosphates. Intracellular NTPDases reside in the lumen of the ER and Golgi, where they participate in the recycling of lumenal UDP and GDP produced during protein glycosylation reactions. In vertebrates, cell surface-located variants have evolved that are responsible for signal degradation in extracellular purinergic signalling by nucleotides. This subgroup (NTPDase1–3 and NTPDase8) is characterized by two transmembrane helices close to the N- and C-termini. Their enzymatic activity has strong implications for vascular haemostasis, immunoregulation, nociception and development (Zimmermann *et al.*, 2012). NTPDases have also been identified in several parasites, including the protozoans *Toxoplasma gondii*, *Trypanosoma* spp., *Leishmania* spp., *Trichomonas vaginalis*, the flatworm *Schistosoma mansoni* and the bacterium *Legionella pneumophila* (Sansom *et al.*, 2007; Sansom, Robson *et al.*, 2008; Krug *et al.*, 2012). It has been suggested that the NTPDase gene of *L. pneumophila* is the result of a horizontal gene transfer (Zimmermann *et al.*, 2012). The function of NTPDases in pathogens remains rather elusive, but they may be involved in the virulence of the

microbes by interfering with the host's immune response or may serve to scavenge adenosine for growth of the microbes (Sansom, Robson *et al.*, 2008; Sansom, 2012). The NTPDase1 of *L. pneumophila* has been shown to be required for multiplication in the replicative vacuole (Sansom *et al.*, 2007).

Vertebrate NTPDases have been shown to be strongly inhibited by low concentrations of several polyoxometallates, albeit with different subtype specificities (Müller *et al.*, 2006). The bacterial enzyme, despite being a close functional homologue with high sequence identity around the active site, was inhibited to a lesser extent, with inhibition constants in the micromolar range (Sansom, Riedmayer *et al.*, 2008).

We have previously determined the structures of the catalytic ectodomains (ECDs) of *Rattus norvegicus* (*Rn*) NTPDase1 and NTPDase2 and determined the disulfide-reductive activation mechanism of the dormant NTPDases of *T. gondii* (Zebisch & Sträter, 2007, 2008; Krug *et al.*, 2012; Krug, Totzauer & Strater, 2013; Krug, Totzauer, Zebisch *et al.*, 2013; Zebisch *et al.*, 2012). The most detailed crystallographic study of NTPDase structure and function to date, using *L. pneumophila* NTPDase1 (Zebisch, Krauss *et al.*, 2013; Zebisch, Schäfer *et al.*, 2013), which shares 21% sequence identity with the vertebrate NTPDase ectodomains, gave insight into the dual specificity mechanism and transition-state stabilization. From structures of *Rn*NTPDase1 in complex with decavanadate and heptamolybdate, a possible inhibitory mechanism of the metal clusters could be proposed: both clusters bind to a loop that is involved in nucleoside recognition (Zebisch *et al.*, 2012). This loop is also the target of an inhibitory antibody against NTPDase3 (Ivanenkov *et al.*, 2010), and in NTPDase2 it undergoes a major conformational change when binding the sulfoanthraquinone inhibitor PSB-071 (Zebisch *et al.*, 2014).

Here, we describe the binding modes of decavanadate, heptamolybdate, octamolybdate and dodecatungstate (POM-1) to *Lp*NTPDase1. Cocrystallization with POM-1 induced a new crystal form with a partially open active-site cleft to which a tartrate ion has bound. Given the highly ordered mode of binding, polyoxometallates may also constitute a general tool for the experimental phase determination of new NTPDase structures that cannot be solved by molecular replacement.

Table 1
Data-collection and refinement statistics.

Values in parentheses are for the outer shell.

	Decavanadate	Hepta/octamolybdate	POM-1
Crystal form	II	II	VI
Position of His tag	C-terminal	C-terminal	N-terminal
X-ray source	Rotating anode	Rotating anode	BESSY BL14.1
Wavelength (Å)	1.5418	1.5418	0.9184
Space group	$P2_1$	$P2_1$	$P6_322$
Unit-cell parameters			
a (Å)	62.4	64.6	143.7
b (Å)	85.8	85.4	
c (Å)	72.3	71.8	75.2
β (°)	106.4	103.9	
Wilson B factor (Å^2)	16.5	12.6	17.5
Resolution range (Å)	29.03–1.69 (1.79–1.69)	45.30–1.49 (1.57–1.49)	29.38–1.70 (1.84–1.70)
Unique reflections	80289 (11303)	119751 (16371)	50327 (7103)
Average multiplicity	7.4 (6.5)	6.1 (4.3)	14.5 (4.3)
Anomalous multiplicity	3.8 (3.4)	3.1 (2.2)	7.6 (2.2)
Completeness (%)	98.8 (95.7)	96.5 (90.5)	99.3 (97.7)
Anomalous completeness (%)	98.1 (90.6)	95.2 (86.2)	99.4 (97.7)
Mean $I/\sigma(I)$	34.3 (7.8)	18.4 (4.2)	18.1 (2.3)
R_{merge} (%)	3.6 (22.5)	6.1 (32.8)	10.3 (56.1)
R_{meas} (all) (%)	4.6 (26.8)	7.8 (42.7)	12.1 (74.0)
$R_{p.i.m.}$ (all) (%)	1.7 (10.2)	2.8 (20.0)	3.0 (35.0)
R_{anom} (%)	2.3 (10.8)	3.0 (21.5)	5.9 (35.1)
Molecules per asymmetric unit	2	2	1
Refinement			
Refinement type	TLS	Anisotropic	Anisotropic
R_{work} (%)	15.9	12.6	14.9
R_{free} (%)	19.2	16.9	19.8
No. of non-H atoms			
Protein	6029	6024	2893
Water	437	464	207
Ligands	181	282	64
Average B factor (Å^2)			
Protein	18.1	16.6	23.5
Water	25.4	28.7	31.1
Ligands	26.2	18.3	33.5
R.m.s.d. from ideality			
Bond lengths (Å)	0.018	0.021	0.014
Bond angles (°)	1.955	2.574	1.420
Ramachandran plot			
Favoured (%)	96.9	97.6	98.1
Allowed (%)	100.0	100	100
No. of outliers	0	0	0
PDB code	4brh	4bvp	4bvo

2. Materials and methods

2.1. Protein preparation and crystallization

The protein used for crystallization was produced, purified and crystallized essentially as described by Zebisch, Schäfer *et al.* (2013). To obtain the structure with molybdate clusters, a crystal of form II was soaked for 4 d in 30 m*M* ammonium heptamolybdate solution. The formation and binding of decavanadate was observed when a crystal of form II was soaked with orthovanadate and thiamine monophosphate to obtain the thiamine phosphovanadate transition-state mimic *in situ* (Zebisch, Krauss *et al.*, 2013). The addition of 10 m*M* POM-1 solution to the *Lp*NTPDase1 enzyme allowed crystallization in a new crystal form (Zebisch, Schäfer *et al.*, 2013).

2.2. Data collection and processing

Cryoprotection and flash-cooling were performed as described with 10 m*M* POM-1 or 15 m*M* ammonium hepta-

molybdate present in the cryobuffer. Data sets were collected on beamline 14.1 at the Protein Structure Factory/Berliner Elektronenspeicherring-Gesellschaft für Synchrotronstrahlung (Berlin, Germany) and on a rotating Cu-anode home source. X-ray data sets were integrated using *XDS* (Kabsch, 2010). Amplitudes were scaled and converted to structure factors with *SCALA*/*CTRUNCATE* (Winn *et al.*, 2011) (Table 1). Structures were solved by molecular replacement using the apo form of *Rn*NTPDase2 (PDB entry 3cj1; Zebisch & Sträter, 2008). Restraints for the metal clusters were generated as described in Zebisch *et al.* (2012).

2.3. Kinetic measurements

Kinetic measurements based on the calorimetric detection of substrate turnover in an isothermal titration calorimetry (ITC) device were performed as described in Zebisch *et al.* (2012) and Zebisch, Krauss *et al.* (2013). Compounds tested for inhibition were added to the enzyme present in the ITC cell as well as to the substrate stock solution in the stirring syringe.

3. Results and discussion

3.1. Binding modes of the metal clusters

To provide additional structural insights into NTPDase inhibition by polymetallate clusters, we solved the structure of *Lp*NTPDase1 in complex with heptamolybdate/octamolybdate, decavanadate and POM-1 dodecatungstate (Table 1). The metal clusters were added during crystallization (POM-1), soaked in (heptamolybdate) or formed spontaneously during soaking with vanadate to obtain a thiamine phosphovanadate transition-state mimic (decavanadate; structure previously published with PDB code 4brh; Zebisch, Krauss *et al.*, 2013) or during soaking with heptamolybdate (octamolybdate).

All clusters bound to *Lp*NTPDase1 in a highly ordered fashion; however, the binding site for heptamolybdate and decavanadate previously identified in *Rn*NTPDase1 is not conserved in *Lp*NTPDase1. In *Lp*NTPDase1, the decavanadate and heptamolybdate clusters are bound deeper in the active-site cleft (Figs. 1 and 2). Crystals soaked with ammonium heptamolybdate (AHM) showed simultaneous binding of an octamolybdate ion in close proximity to the heptamolybdate (Figs. 2*b*, 2*c* and 2*d*). Binding of octamolybdate and heptamolybdate has induced a structuring of the hexahistidine tag of a neighbouring molecule that is normally flexible. One of the histidine residues is coordinated to a molybdenum(VI) of the octamolybdate. In addition to the large molybdate clusters and a distorted orthomolybdate ion in the terminal phosphate-binding site (Zebisch, Krauss *et al.*, 2013), we observe high-occupancy binding of two dimolybdate and one trimolybdate species per monomer. These smaller species bound covalently to amide and acid side-chain functionalities at the protein surface distant from the active site (not shown). The multitude of bound oligomolybdate species including the octamolybdate is likely to have resulted from impurities and interconversion from heptamolybdate during the prolonged four-day soaking.

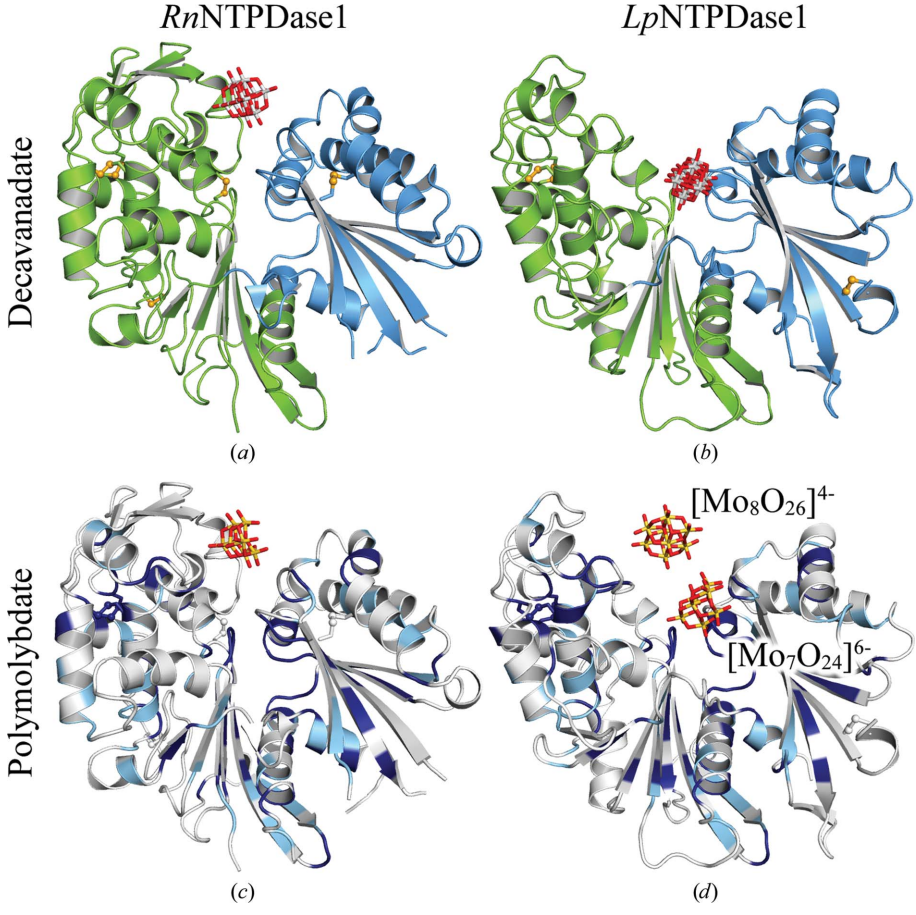

Figure 1
Comparison of the binding sites of decavanadate (*a*, *b*) and polymolybdate (*c*, *d*) clusters in *Rn*NTPDase1 and *Lp*NTPDase1. The cartoon drawing has been coloured based on domains in (*a*) and (*b*) and based on sequence identity (blue) and similarity (pale blue) between the two NTPDases in (*c*) and (*d*).

3.1.1. Octamolybdate. The octamolybdate binds at a crystal contact between two monomers (Figs. 2*b* and 2*c*). In addition to the covalently bound histidine from the affinity tag, a covalent bond is formed to Ser127 in the N-terminal domain. Hence, the formation of the octamolybdate may have been induced or supported by the crystal packing. However, the highly ordered and almost fully occupied binding mode itself is very surprising.

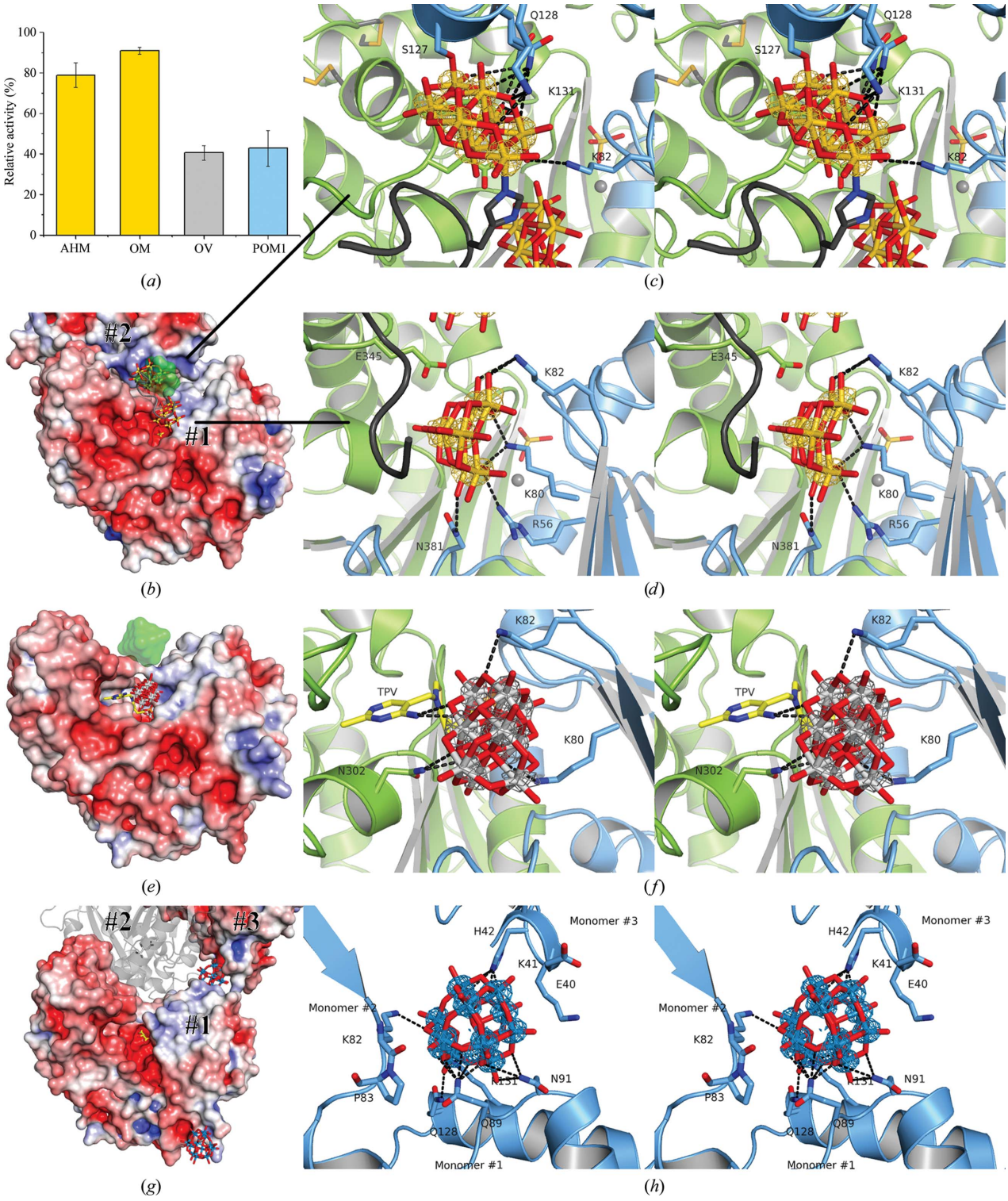

Figure 2
(*a*) Inhibition of *Lp*NTPDase1 by metallate compounds. Relative ADPase activity with 1.5 m*M* substrate and 500 µ*M* metallate compound. OM, sodium orthomolybdate; OV, sodium orthovanadate. The activity in the absence of inhibitor (100%) is 1134 ± 41 µmol min^{-1} mg^{-1}. (*b*)–(*h*) Binding modes of the metal clusters to *Lp*NTPDase1. Left, protein surface coloured by the electrostatic potential; right, close-up views showing anomalous density maps contoured at 5σ. (*b*)–(*d*) In an ammonium heptamolybdate-soaked crystal, binding sites for heptamolybdate and octamolybdate were identified. The binding site of the octamolybdate (*c*) overlaps with the heptamolybdate binding site identified in *Rn*NTPDase1 (green in *b*). Binding of the metal clusters has led to structuring of a His tag of an adjacent molecule (black). The octamolybdate ion has bound between the two monomers of the asymmetric unit. Two covalent bonds between protein and metal cluster have formed *via* ligand exchanges of nonbridging O atoms. One is to Ser127 and one is to a His-tag histidine of a symmetry-related monomer. (*d*) Apart from the His tag, the heptamolybdate binds to the active-site cleft of a single monomer. (*e*, *f*) The decavanadate anion binds in the active-site cleft. The base of the thiamine phosphovanadate (TPV) adduct interacts with the decavanadate ion *via* two hydrogen bonds. The binding site of decavanadate to *Rn*NTPDase1 is indicated in green in (*e*). (*g*, *h*) The dodecatungstate anion POM-1 binds at a crystal contact between two N-terminal domains. A tartrate ion can be identified in the active site.

Also, the binding site of heptamolybdate in *Rn*NTPDase1 overlaps with this site (Fig. 2*b*).

3.1.2. Heptamolybdate. Apart from the structured His tag, the heptamolybdate ion only binds to a single protein monomer. It forms hydrogen bonds to three positively charged residues of the N-terminal lobe and one C-terminal asparagine residue that can also be ascribed to this domain (Zebisch, Krauss *et al.*, 2013). Of these, Arg56 was shown to be involved in substrate binding and to be indispensable for activity (Zebisch, Krauss *et al.*, 2013). Hence, aspects of a competitive inhibition mode are immediately inferable from this binding mode. Lys80 and Lys82 are also involved in decavanadate binding (see below).

Surprisingly, we found only weak inhibition of the *Lp*NTPDase1 ADPase activity by ammonium heptamolybdate, which is a strong inhibitor of *Rn*NTPDase1 (Fig. 2*a*). Similarly, almost no inhibition was observed in kinetic assays with orthomolybdate, although it binds to the catalytic centre in a distorted transition state-like manner (Zebisch, Krauss *et al.*, 2013). Fig. 3 shows that no clashes would occur upon simultaneous binding of ADP and heptamolybdate, suggesting that the weak inhibition might indeed be caused only by the recruitment of the catalytic Arg56 side chain. More clashes could be expected from a GDP substrate, whose transition-state mimic guanosine 5′-phosphovanadate (GPV) displays a shifted base binding mode (PDB entry 4brl; Zebisch, Krauss *et*

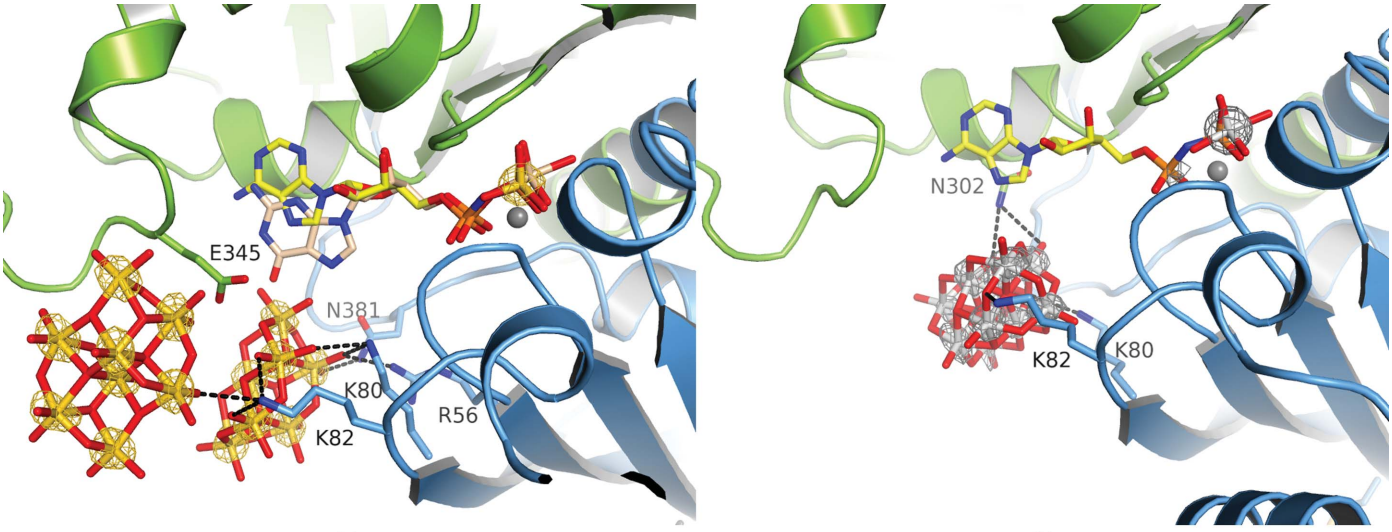

Figure 3
Comparison of the binding sites of substrate analogues and metal clusters in the active-site cleft. (*a*) The polymolybdate complex superimposed with the ADP analogue AMPNP (PDB entry 4brc, yellow) and the GDP transition-state mimic GPV (PDB entry 4brl, wheat). (*b*) The decavanadate complex superimposed with the ADP analogue AMPNP.

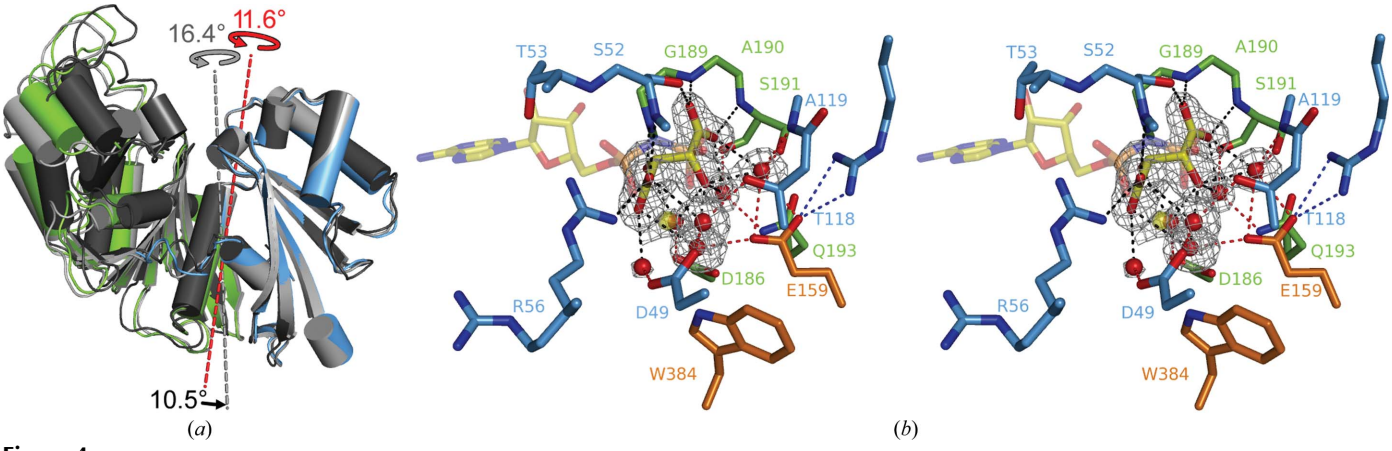

Figure 4
The POM-1-induced new crystal form. (*a*) Domain orientation of *Lp*NTPDase1 in the POM-1 complex structure. The structure (coloured) is compared with the most open apo structure (light grey, PDB entry 4br4) and the closed-state Mg^{2+}/AMPNP complex (dark grey, PDB entry 4br6). To transition to the closed state, one domain needs to rotate 11.6° around the axis shown in red. The rotation axis describing the transition from the most open to the closed structure is shown in grey. (*b*) Tartrate binding to the active site of *Lp*NTPDase1. The tartrate ion in the active site occupies the phosphate binding sites of the substrate in the absence of metal ion and forms similar hydrogen bonds. The OMIT density of ligand and waters is contoured at 3σ. The binding mode of an Mg^{2+}/AMPNP complex of the closed state copied from a superposition using the C-terminal domain only is shown in half transparency. Residues involved in hinge formation of the domain closure are shown in orange.

al., 2013). Yet, for GDP hydrolysis we also only observed an inhibition of 17 ± 3%.

3.1.3. Decavanadate. The decavanadate cluster formed *in situ* binds together with a thiamine phosphovanadate transition-state mimic to the active-site cleft of *Lp*NTPDase1 (structure previously published with PDB code 4brh; Zebisch, Krauss *et al.*, 2013) and occupies a similar binding site as the heptamolybdate cluster described above. It is contacted by residues from both domains (Figs. 2*e* and 2*f*). Apart from this small number of direct polar interactions, it seems that it is rather a certain shape complementarity that favours binding in this specific orientation. Based on superpositions with ADP (Fig. 3*b*) and ATP complexes (not shown), no strong competitive inhibition by a stable inhibitor isosteric to decavanadate would be expected. However, the thiamine group of the transition-state mimic appears to support the formation and binding of the decavanadate cluster. With other NDPase transition-state mimics generated *in situ* in an analogous fashion, no binding (GMP/VO_4^{3-}; PDB entry 4brl) or only very poor binding (AMP/VO_4^{3-}; PDB entry 4bre) was observed (Zebisch, Krauss *et al.*, 2013). This leads to the assumption that metal clusters might be found that selectively inhibit NTPDase turnover of specific substrates. Except for the vanadate moiety in the transition-state mimic (Zebisch, Krauss *et al.*, 2013), no further vanadate binding sites could be identified based on anomalous Fourier transform peaks. Owing to its inherent instability and non-quantitative formation at neutral pH, an intrinsic problem to the use of polymetallates as enzyme inhibitors, decavanadate is not amenable for inhibition studies. We find that orthovanadate alone has a pronounced effect on the activity (Fig. 2*a*).

3.1.4. Dodecatungstate. The spherical polytungstate cluster POM-1 bound at the interface between three symmetry mates (Figs. 2*g* and 2*h*). All binding sites are distant from the active site and a direct impact on activity is not obvious. Yet, we could not identify any additional weak binding sites that would have revealed themselves in anomalous density maps. This, together with the fact that the compound was used in cocrystallization at a high excess over the published K_i value of 267 µ*M*, suggests that one of the binding sites is the one underlying inhibition (Fig. 2*a*). We speculated that POM-1 might stabilize a weakly populated dimer of *Lp*NTPDase1 that persists in all six crystal forms described to date (Zebisch, Krauss *et al.*, 2013; Zebisch, Schäfer *et al.*, 2013). By cross-linking the two monomers (labelled #1 and #2 in Figs. 2*b*, 2*g* and 2*h*), a domain motion required for catalysis might be impaired (see also below). However, we could not establish stable POM-1-induced dimerization using gel filtration (data not shown). We suppose that the inhibitory effect results from destabilization of the enzyme structure in solution.

Taken together, the three tested metal clusters show surprisingly well defined binding modes. While a competitive inhibition mechanism is not inferable for POM-1, this might be the case for decavanadate and heptamolybdate. At least for heptamolybdate, participation of the catalytic side chain of Arg56 in cluster binding was observed. However, inhibition by heptamolybdate seems to be low. Compared with the ECDs of *Rn*NTPDase1 and *Rn*NTPDase2, *Lp*NTPDase1 has a lower isoelectric point, which is reflected by a more negative surface potential of the active-site cleft. Nevertheless, the cleft is lined by several positively charged side chains mostly originating from the N-terminal domain, which may serve to

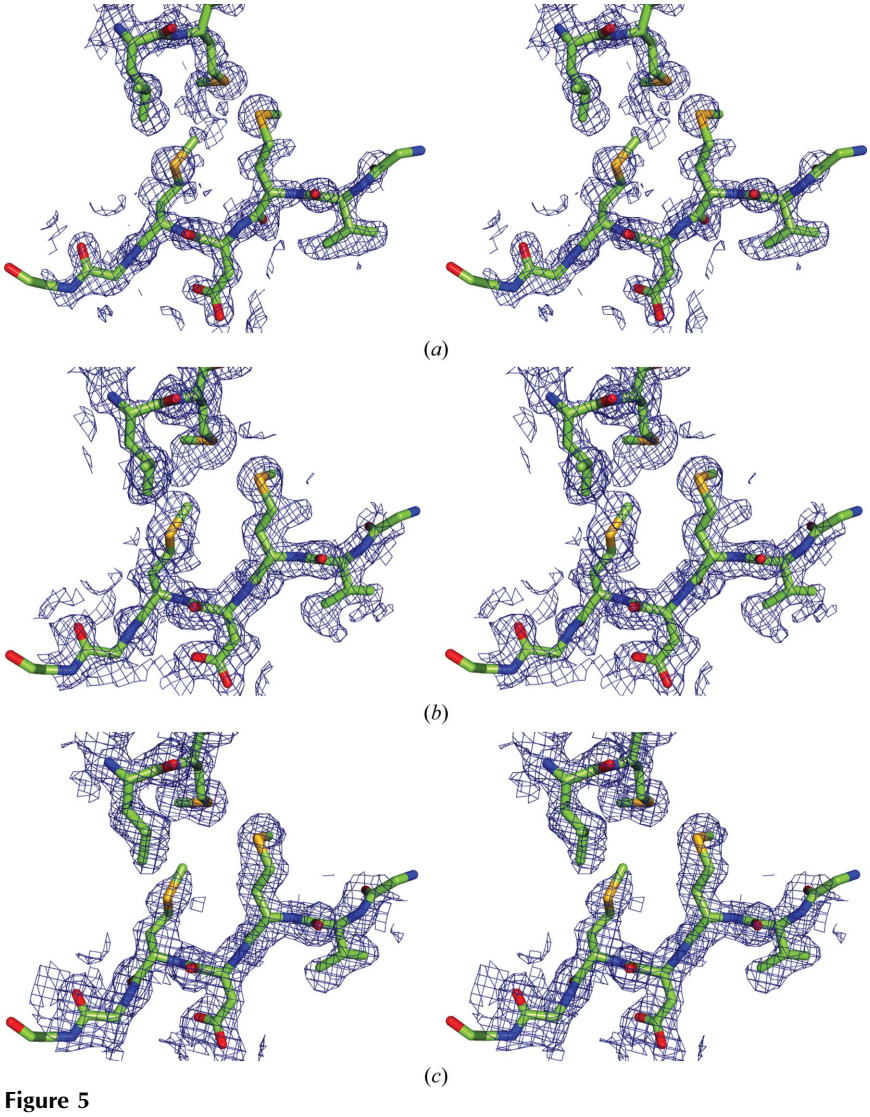

Figure 5
Representative experimental electron density after after SAD phasing and phase refinement by solvent modification (see text for details) contoured at 1σ. Heavy-atom search and phasing of crystals soaked with ammonium heptamolybdate (*a*) and vanadate (*b*) or co-crystallized with POM-1 dodecatungstate (*c*) was performed with *Phaser-EP*.

lead the nucleotide substrate into the active site, where it is then bound as the metal–nucleotide complex. Apparently, some metal clusters have the ability to fit into the active-site cleft and bind to these residues. This would allow them to block substrate entrance to the active-site cleft. The binding mode of decavanadate in the presence of a transition-state mimic shows that uncompetitive inhibition is also possible. The binding may be further stabilized by binding to functionalities of the bound substrate or product.

3.2. The POM-1 metal cluster stabilizes a half-open conformation

Recently, based on crystallographic observations of closed and open states, we were able to describe the domain rotation of *Lp*NTPDase1 in great detail (Zebisch, Krauss *et al.*, 2013). Analysis of the new crystal form obtained only in the presence of POM-1 shows that the crystal contacts induced by POM-1 stabilize an intermediate open conformation (Fig. 4*a*). A domain rotation of 11.6° around the axis shown in red was calculated for the transition from the new structure to the closed state described previously (Zebisch, Krauss *et al.*, 2013). With the rotation axis inclined only 10.5° from that calculated for the transition from the most open to the closed state, it is clear that the new conformation is on the path of the described domain closure. We have described intermediate open conformations of *Lp*NTPDase1 before, but these structures suffered from twinning and lower resolution (Zebisch, Schäfer *et al.*, 2013).

3.3. A tartrate ion occupies the canonical phosphate binding sites

In the POM-1 complex of *Lp*NTPDase1, the active-site cleft harbours a tartrate ion (Fig. 4*b*). The dicarboxylate occupies the binding site for the pyrophosphate tail of the substrate. Many hydrogen bonds that are normally formed between the substrate and the proton donors of the phosphate-binding loops are also satisfied by tartrate. However, no hydrogen bonds are formed to Thr53 of the apyrase conserved region (ACR) 1 and Thr118 of ACR 2. The side chain of Arg56 is observed in two conformations, of which only one participates in tartrate binding. The finding that the phosphate tail can be mimicked by oligocarboxylic acids might be useful in future fragment-based and structure-based drug-design efforts. Notably, the tartrate ion binds in the absence of the catalytic divalent metal ion, which is replaced by a water molecule.

3.4. Metal clusters as SAD phasing tools

The metal-cluster complex structures described here were solved by molecular replacement. Nevertheless, we noticed a strong anomalous signal in all three data sets, indicated by a high $R_{\rm anom}$ value that exceeds the redundancy-corrected $R_{\rm p.i.m.}$ value (Table 1). Based on the notion that the described metal clusters might also bind to novel NTPDase crystals in a highly ordered fashion, we wondered whether it was possible to solve the structures from the SAD data sets alone. Indeed, we found that it was possible to solve the structure of *Lp*NTPDase1 from all three data sets when the *Phaser* SAD pipeline in *CCP*4 (Read *et al.*, 2013) was instructed to search for the appropriate number of heavy atoms.

For the POM-1 structure 26 sites were found (12 searched), which all clustered around the 12 genuine tungstate sites of the cluster. The figure of merit (FOM) was 0.464 (0.494/0.213 acentric/centric) before solvent modification and 0.651 for the correct hand after solvent modification with *Parrot*. To phase the decavanadate complex for which data were collected at the Cu $K\alpha$ wavelength, we searched for 22 sites (two clusters and two hydrolytic site single vanadate ions). 62 heavy-atom sites were found, which included not only all the vanadate sites but also sulfur and phosphate atoms. The FOM was 0.361 (0.370/0.153 acentric/centic) before solvent modification and 0.672 after solvent modification. In the case of the heptamolybdate-soaked crystal, 83 sites were found (16 searched) which again included several correct sulfur positions. The FOM was 0.585 (0.592/0.497 acentric/centric) before solvent modification and 0.586 after solvent modification, highlighting the excellence of the purely experimental phases. In all three cases the electron density was immediately traceable, revealing even well defined side-chain conformations (Fig. 5). The highly ordered binding mode of metal clusters to NTPDases as observed here and in rat NTPDase1 (Zebisch *et al.*, 2012) hence make them a premium choice as phasing tools for new NTPDase structures. For lower resolution structures it might be sensible to specify a cluster search as implemented in *Phaser* SAD.

The Deutsche Forschungsgemeinschaft (DFG) is acknowledged for financial support of this project under grant STR 477/10. We thank PSF/BESSY of the Helmholtz-Zentrum Berlin and EMBL/DESY (Hamburg) for beam time and travelling support and the staff for support at the beamlines. We want to thank Peter Lauble, Christian Roth and Michael Zahn for their support. Ulrike Krug is acknowledged for discussion.

References

Ivanenkov, V. V., Crawford, P. A., Toyama, A., Sévigny, J. & Kirley, T. L. (2010). *Protein Eng. Des. Sel.* **23**, 579–588.
Kabsch, W. (2010). *Acta Cryst.* D**66**, 125–132.
Krug, U., Totzauer, R. & Sträter, N. (2013). *Proteins*, **81**, 1271–1276
Krug, U., Totzauer, R., Zebisch, M. & Strater, N. (2013). *ChemBioChem*, **14**, 2292–2300.
Krug, U., Zebisch, M., Krauss, M. & Sträter, N. (2012). *J. Biol. Chem.* **287**, 3051–3066.
Müller, C. E., Iqbal, J., Baqi, Y., Zimmermann, H., Röllich, A. & Stephan, H. (2006). *Bioorg. Med. Chem. Lett.* **16**, 5943–5947.
Read, R. J., Adams, P. D. & McCoy, A. J. (2013). *Acta Cryst.* D**69**, 176–183.
Sansom, F. M. (2012). *Parasitology*, **139**, 963–980.
Sansom, F. M., Newton, H. J., Crikis, S., Cianciotto, N. P., Cowan, P. J., d'Apice, A. J. & Hartland, E. L. (2007). *Cell. Microbiol.* **9**, 1922–1935.
Sansom, F. M., Riedmaier, P., Newton, H. J., Dunstone, M. A., Müller, C. E., Stephan, H., Byres, E., Beddoe, T., Rossjohn, J., Cowan, P. J., d'Apice, A. J., Robson, S. C. & Hartland, E. L. (2008). *J. Biol. Chem.* **283**, 12909–12918.
Sansom, F. M., Robson, S. C. & Hartland, E. L. (2008). *Microbiol. Mol. Biol. Rev.* **72**, 765–781.

Winn, M. D. *et al.* (2011). *Acta Cryst.* D**67**, 235–242.
Zebisch, M., Baqi, Y., Schäfer, P., Müller, C. E. & Sträter, N. (2014). *J. Struct. Biol.* **185**, 336–341.
Zebisch, M., Krauss, M., Schäfer, P., Lauble, P. & Sträter, N. (2013). *Structure*, **21**, 1460–1475.
Zebisch, M., Krauss, M., Schäfer, P. & Sträter, N. (2012). *J. Mol. Biol.* **415**, 288–306.
Zebisch, M., Schäfer, P., Lauble, P. & Sträter, N. (2013). *Acta Cryst.* F**69**, 257–262.
Zebisch, M. & Sträter, N. (2007). *Biochemistry*, **46**, 11945–11956.
Zebisch, M. & Sträter, N. (2008). *Proc. Natl Acad. Sci. USA*, **105**, 6882–6887.
Zimmermann, H., Zebisch, M. & Sträter, N. (2012). *Purinergic Signal.* **8**, 437–502.